J Mater Sci (2006) 41:7498–7505
DOI 10.1007/s10853-006-0833-x

The influence of porosity on the fatigue crack growth behavior of Ti–6Al–4V laser welds

L. W. Tsay · Y.-P. Shan · Y.-H. Chao · W. Y. Shu

Received: 23 December 2004 / Accepted: 7 November 2005 / Published online: 4 October 2006

Abstract The effect of porosity—a common welding defect—on the fatigue crack growth rate (FCGR) in Ti–6Al–4V laser welds was investigated. The experimental results reveal that porosity was present in partial penetration welds over a narrow fusion zone (FZ) with martensite structure. The FCGR of the FZ was lower than that of the base plate. The fracture surface morphology of weld metal was much rougher as compared to that of the base plate. Randomly oriented martensite in the FZ led to local cleavage fracture along a preferred plane, thus, altering the crack growth direction significantly out of the primary crack plane. The zigzag crack path in the FZ resulted in a reduced FCGR at a given ΔK compared to the base plate. Besides, the porous weld showed a serration on the crack growth curve, and behaved the similar crack growth characteristics as the defect free one. SEM fractography revealed that the deflection of crack path around porosity together with local notch blunting as the crack tip pierced into porosity, balanced the increased FCGR for the occurrence of instant crack advance as the crack front reached the porosity at a low stress ratio. In contrast, the serration and drop in FCGR occurred sparingly at a high stress ratio as the crack front met the porosity.

L. W. Tsay (✉) · Y.-P. Shan
Institute of Materials Engineering, National Taiwan Ocean University, Keelung 202, Taiwan, R.O.C.
e-mail: b0186@mail.ntou.edu.tw

Y.-H. Chao
Department of Mechanical Engineering, National Taiwan Ocean University, Keelung 202, Taiwan, R.O.C.

W. Y. Shu
Chung Shan Institute of Science and Technology, Lungtan 325, Taiwan, R.O.C.

Introduction

Titanium alloys have been widely used in the aerospace industries in view of its remarkable strength to weight ratio. Excellent corrosion resistance in aqueous solution, especially in chloride solution, also makes them as candidate materials for marine and chemical applications. Amongst various titanium alloys, Ti–6A1–4V is one of the most important titanium alloys used in distinct fields for its high specific strength and excellent corrosion resistance. Inert gas arc welding processes is traditionally used to assemble components and/or piping system made of titanium alloys [1]. However, laser beam welding can produce a weld with a high depth-to-width ratio and a narrow HAZ [2]. Meanwhile, the ease of automation makes it widely used to improve productivity in various applications [3, 4]. Therefore, traditional arc welding of titanium alloys have been replaced gradually by laser welding.

In these days, laser welding is a mature technology to produce high quality welds which are comparable in quality with those of electron beam (EB) welds. Because of the high temperature reactivity of titanium alloys, EB welding is the most popular method for joining Ti–6Al–4V with high quality [5]. Nowadays, laser beam welding has been proven to be able to provide welds of similar quality as compared to those

of EB welds [6]. However, laser welding under improper conditions can result in introduction of a large amount of porosity into the fusion zone (FZ) [7]. Hydrogen-induced porosity is characterized by small blow holes and is a serious problem in laser welding of Al-alloys [7]. The intense metal vapor together with entrapped gas and air leads to the instability of welding keyhole, and as a consequence, the bubble is trapped by solidifying metal resulting in the formation of large porosity [7]. Moreover, the quality of titanium weld is affected greatly by the presence of impurities in the FZ. Contamination by interstitial elements such as O, N can decrease the tensile ductility of the weld metal [8]. It was found that no significant oxygen contamination occurred in laser welding under effective shielding [9]. Also, removal of titanium oxide from the surface by chemical etching prior to welding does not affect the oxygen content in the titanium welds [10].

Titanium alloys are frequently used as primary structures and dynamically loaded components, therefore, fatigue crack growth behavior of Ti–6A1–4V alloy has been studied extensively. Fatigue crack growth rate (FCGR) for this alloy is influenced by microstructures [11–14], environment [15–19] and interstitial content of the alloy [15, 20]. The effect of microstructure on the fatigue crack growth behavior is related to the role of crack path morphology that causes crack closure and crack deflection [21]. In the open literatures, relatively few works have been focused on investigating the fatigue crack growth behavior of Ti–6Al–4V welds, and much less study concerning the effect of porosity on the fatigue properties of weld metal. The aim of the present work is to investigate the effect of microstructures and weld porosity on the fatigue crack growth behavior of Ti–6Al–4V laser weld. Fatigue-fractured appearance was examined and paid special attention on the deflection of crack path and changes in the fracture mode.

Material and experimental procedures

The chemical composition of the 4.0 mm thick Ti–6A1–4V alloy by weight percentage is 6.20 A1, 4.22 V, 0.14 Fe, 0.019 C, 0.014 O and balanced Ti. The tensile properties of the as-received material are: ultimate tensile strength—1005 MPa, yield strength—910 MPa and elongation—20%. The microstructure of the as-received Ti–6Al–4V plate consisted of a small percentage of β phase distributed at the elongated α grain boundary. All specimens were welded in the as-received condition with the welding direction normal to the rolling direction. A Rofin-Sinar RS 850 – 5 kW CO_2 laser was utilized for laser welding. Table 1 lists the parameters used for laser welding of test coupons in this study. Post-weld heat treatments (PWHTs) were performed on the welds over the temperature range of 482–593 °C (900–1100°F) for 3 h in vacuum followed by Ar assist cooling to room temperature. Specimens were identified based on the processing parameters. For the post heat-treated weld, the last 3 digits represented the aging temperature.

Table 1 Laser welding parameters used in the experimental

Focal lens	Cu mirrior
Focal length	200 mm
Focal point	0.5 mm below the surface
Plasma-assisted gas flow rate	30 L/min He
Shielding gas flow rate	15 L/min Ar
Backing gas flow rate	10 L/min Ar

Three different types of laser welds were fabricated corresponding to the depth of penetration. The full penetration weld (FW) had been performed by welding in one pass at the laser power of 3.2 kW and scanned at the rate of 800 mm/min. After X-ray examination, the FW specimen was free of porosity in the FZ. In order to introduce porosity into the FZ, incomplete penetration of the laser weld had been made. Generally, most of the porosity will be formed near the root of the weld. Controlling the depth of penetration by varying the laser scan rate during welding could achieve such an object. While maintaining the laser power at 2 kW, varying the welding speed from 1200 mm/min to 2500 mm/min resulted in a change in penetration depth from 3/4 to 1/2 thickness of the plate, which was named as intermediate penetration weld (IW) and half penetration weld (HW) respectively. In case of the incomplete penetration weld, symmetrical welding on the top and bottom sides of the specimen's surfaces was made to get a through thickness FZ and entrap porosity within the weld metal. After X-ray examination, the quality of the laser weld with lots of fine porosity fell on the rank of class C according to the aerospace material specification AMS-STD-2219A [22].

Compact tension (CT) specimen was used for the fatigue crack growth tests in this work. The fatigue crack growth tests were carried out on a computerized servo-hydraulic MTS testing machine at room temperature. Testing software (790.40 fatigue crack growth) provided by MTS company was used to assist automatic crack growth testing. It offers various testing conditions including constant load, constant K and K-controlled tests. The experimental procedures met the standard of ASTM E647-91 specification. A

constant amplitude load cycling under a sinusoidal waveform of 20 Hz was applied for the fatigue test. Furthermore, the stress ratio (R) of the fatigue test was set either at 0.1 or 0.5. The crack growth direction was aligned parallel to the FZ in the welded CT specimens. Crack length was determined by compliance function [23] and confirmed by a 30× traveling microscope. The results presented here were typical of the experimental data.

Micro-hardness measurements and metallographic observations were undertaken across the weld to compare hardness variations in the FZ, heat-affected zone (HAZ) and unaffected base metal (BM). Fatigue-fractured morphology of various specimens was examined by a scanning electron microscope (SEM). Special attention was paid to those regions showing changes of fracture modes. Fracture surface profile was examined near the mid-section of the specimen in the direction of crack growth using the trace function of the SEM to reveal the variation of surface roughness.

Results and discussion

Figure 1 shows the macroscopic appearance of various welds with micro-hardness distribution. The low heat input of laser welding ensured a narrow FZ and HAZ zones for all welds, particularly for the HW specimen. The results indicated the FZ of FW specimen (Fig. 1a) consisted of the coarse columnar structure relative to other specimens. In contrast, the HW specimen (Fig. 1c) had the finest microstructure among all specimens, which was associated with the lowest energy input during welding. Regardless of welding conditions, the FZ had higher hardness than other regions of a weld. Moreover, the HW specimen behaved the highest FZ hardness among welds. It was deduced the relatively coarse dendrite in the FZ of FW specimen could result in inferior strength. Metallographic observations (not shown here) revealed that the FZ comprised of acicular α' martensite instead of the banded α with intergranular β of the base plate. Rapid cooling of the molten pool during solidification enhanced the formation of martensite in the FZ of a laser weld. The presence of martensite in the FZ was responsible for the increased hardness therein, in spite of welding conditions. The results of previous work demonstrated that the hardness of the FZ could be raised slightly after PWHT [24]. The slight increase in hardness in the FZ was attributed to the decomposition of α‘ martensite to form refined α plus β. Additionally, aging in the temperature range of 500–600 °C led to little influence on the FZ hardness [24].

The FCGR (da/dN in mm/cycle) versus stress intensity factor range (ΔK in MPa $\sqrt{m}$) for various specimens at R ratio of 0.1 or 0.5 is shown in Fig. 2. As the crack propagated within the FZ of defect free welds, the FCGR of the FZ was significantly lower than that of the base plate (Fig. 2a), especially for the weld aged at 482 °C, i.e., FW482 specimen. The retarded crack growth in the FZ of Ti–6Al–4V laser weld is most significant among various regions [24]. The results of this work implied that the aged martensite structure had a higher resistance to crack growth compared to a banded structure in a Ti–6Al–4V alloy. As can be seen in Fig. 2a, the initial resistance to crack growth for FW482 specimen was higher than that for the FW593. In case of the as-welded specimen, it was difficult to pre-crack the specimen at an applied maximum stress intensity factor (K_{max}) below 14 MPa $\sqrt{m}$. K_{max} required to pre-crack the specimen in as-welded condition was observed to be much higher than that in the aged ones. It is known that the fatigue crack growth behavior of the material will be influenced by a combined effect of the material microstructure and residual stress field simultaneously. As could be inferred from the crack growth rate results between FW482 and FW593 specimens, microstructural effect was not predominant on the FCGR. The distribution of residual stress around the narrow FZ of laser weld with irregular appearance was hard to measure by experimental methods. The partial relief and redistribution of residual stresses during crack growth of laser-treated AISI 304 stainless steel have been determined by computer simulation and experimental measurements [25, 26]. The improved crack growth resistance of the specimens in the low ΔK range has been accounted for the presence of residual compressive stress field ahead of crack tip [25–27]. Moreover, the retardation of crack growth within the FZ or HAZ is also attributed to the presence of residual stress ahead of crack tip as the crack propagates in a direction parallel to the welding direction [28, 29]. The observed lower FCGR in the low ΔK range of FW482 specimen as compared to FW593 could be partly attributed to the incomplete stress relief during aging.

Fatigue crack growth behaviors of porous welds relative to the defect free weld all aged at 593 °C are shown in Fig. 2b. IW and HW specimens were known to possess varying levels of porosity, and exhibited the similar FCGR as the defect free weld. Generally, the results indicated the influence of fine porosity on the FCGR of Ti–6Al–4V laser weld was minor. Moreover, porous weld showed a serration on crack growth curves. This could be attributed to the interaction of crack tip with internal porosity, resulting in local

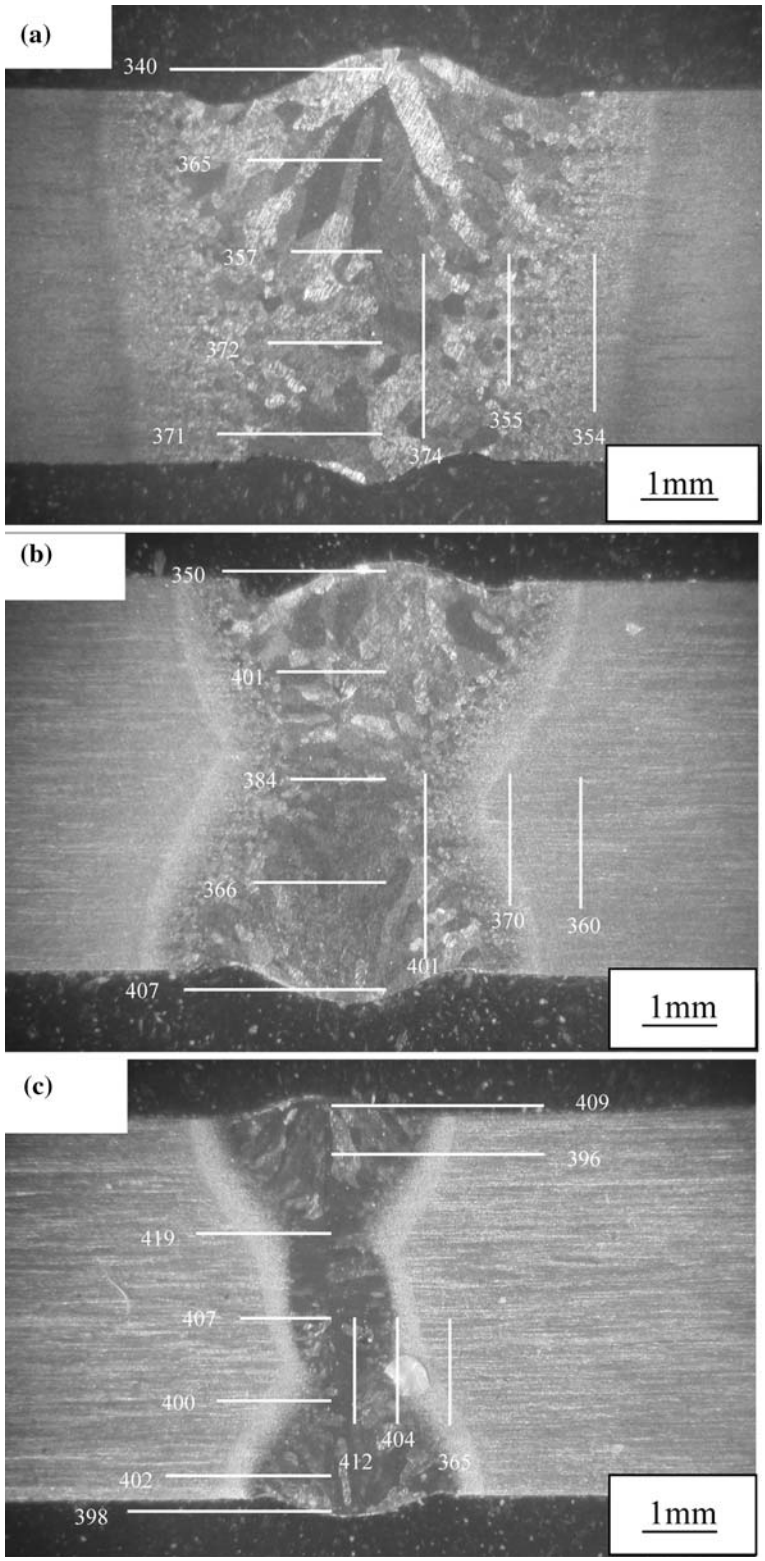

Fig. 1 Macrographs of various Ti–Al6–4V laser welds with micro-hardness distribution for the (**a**) FW, (**b**) IW and (**c**) HW specimens in the as-welded condition

variation of crack driving force and the FCGR; this aspect would be discussed later. It was worth mentioning that sometimes the fatigue crack was found to bypass the porosity, and finally revealed the FCGR close to a defect free weld. This evidence confirmed that the presence of fine porosity in the laser weld might not deteriorate its crack growth behavior greatly. Increasing the stress ratio to 0.5, the rise in FCGR for all the specimens had been found (Fig. 2c). However, all the welds still had a slightly better resistance to

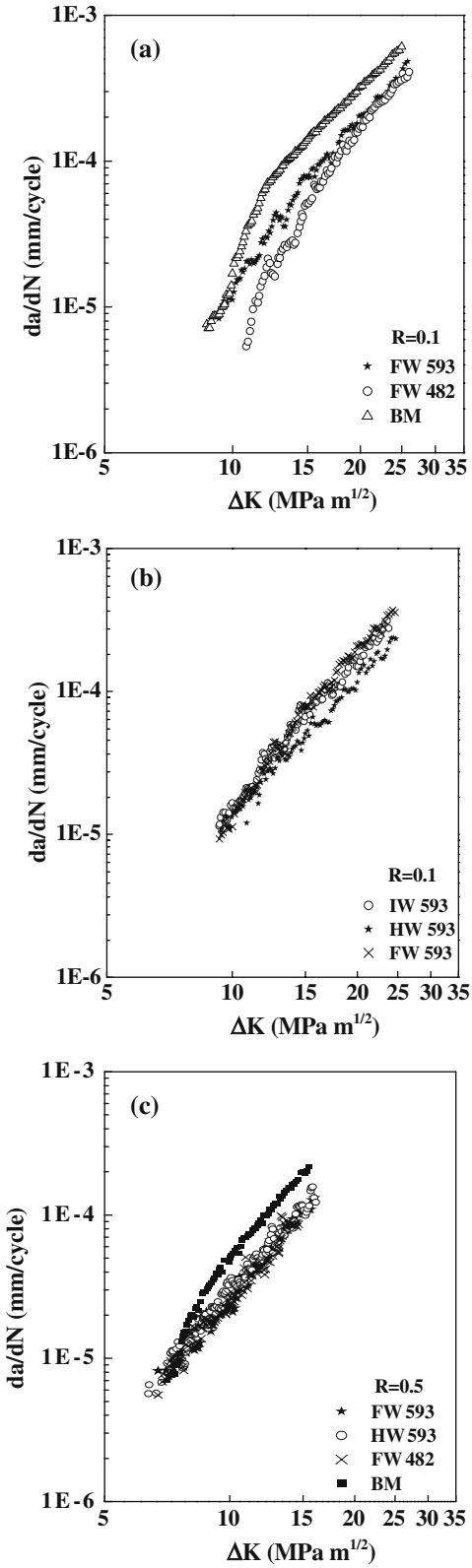

Fig. 2 Variation of crack growth rate (da/dN) versus stress intensity factor range (ΔK) for the specimens, (**a**) 482 and 593 °C aged FW specimen in comparison with base metal testing at R 0.1, (**b**) IW and HW relative to FW welds, all aged at 593 °C testing at R 0.1, (**c**) aged and porous welds as compared to base metal testing at R 0.5

crack growth than the base metal. The results also indicated that the abrupt changes in FCGR for the HW specimen in the low ΔK range were less likely to occur. Furthermore, fatigue-testing at the R of 0.5, FW 482 specimen exhibited similar crack growth characteristics as the FW 593. This implied that the presence of residual stresses had less influence on the FCGR under high R ratio.

Typical macroscopic fatigue-fractured appearance of the base plate and 593 °C aged welds is shown in Fig. 3. Macro-fracture surface morphology of the base plate clearly indicated the strip-like separation (Fig. 3a). This was attributed to de-cohesion along the α/β interfaces in the base plate. It is pointed out that hydrogen segregates to the α/β interfaces, thus resulting in inducing intergranular fracture of Ti–6Al–4V alloy consisting of continuously intergranular β phase [30]. Fatigue-fractured surface of the welds was rather irregular and coarse in features, indicating a typically solidified dendrite structure in the FZ (Fig. 3b–d). Additionally, the surface morphology of welds was much rougher than that of the base plate. A rough

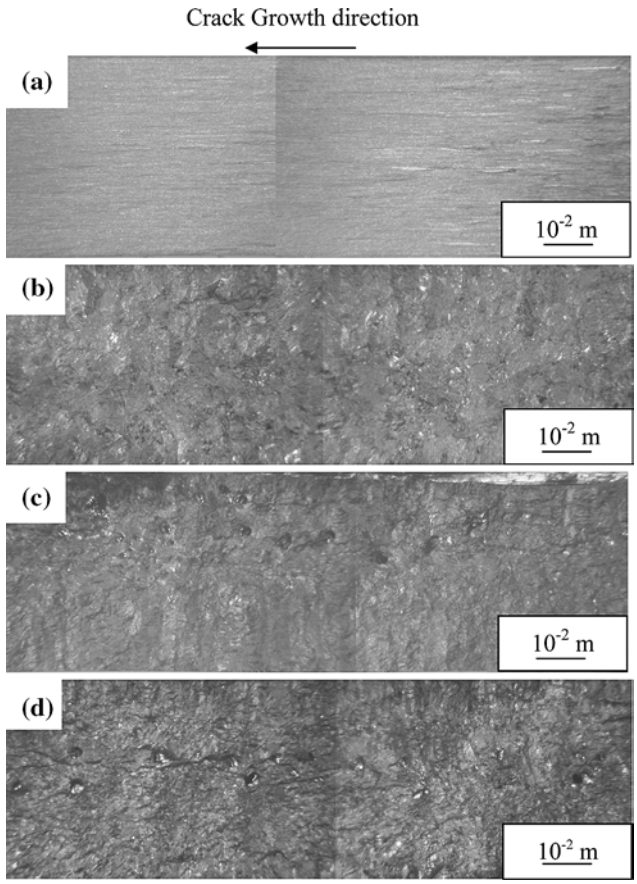

Fig. 3 Typically macroscopic fatigue-fractured appearance of the (**a**) BM, (**b**) FW, (**c**) IW and (**d**) HW specimens aged at 593 °C

fracture surface was expected to lead to high levels of crack closure. The zigzag crack path in the FZ in contrast to the straight path in the base plate could be due to the influence of microstructure—randomly oriented martensite in contrast to banded α/β structure. In case of porous welds, the irregular fracture surface was inter-dispersed with porosity, as shown in Fig. 3c, d. The open porosity located mainly in the mid-thickness of the HW specimen and over 1/2 to 1/4 thickness of the IW specimen.

Figure 4 shows the variation of FCGR versus crack length with photographs showing the location of porosity for HW 593 specimen. Local interaction of the crack tip with porosity led to the serration in macroscopic crack growth curve as the crack front pierced into the weld defect. It appeared that the region with large porosity or agglomeration of individual fine porosity resulted in the change of FCGR under R 0.1, especially in the low ΔK regime. Increasing the R ratio to 0.5, such a drop of FCGR was less likely to occur as the crack propagated along the porous FZ. Regardless of testing conditions, the porosity did not accelerate the crack growth greatly for the entire regime of crack growth investigated. It was deduced that the local rise in crack tip radius as the segment of crack front penetrated into the round porosity led to slow down the FCGR at R 0.1. In case of R 0.5, persistent tensile load

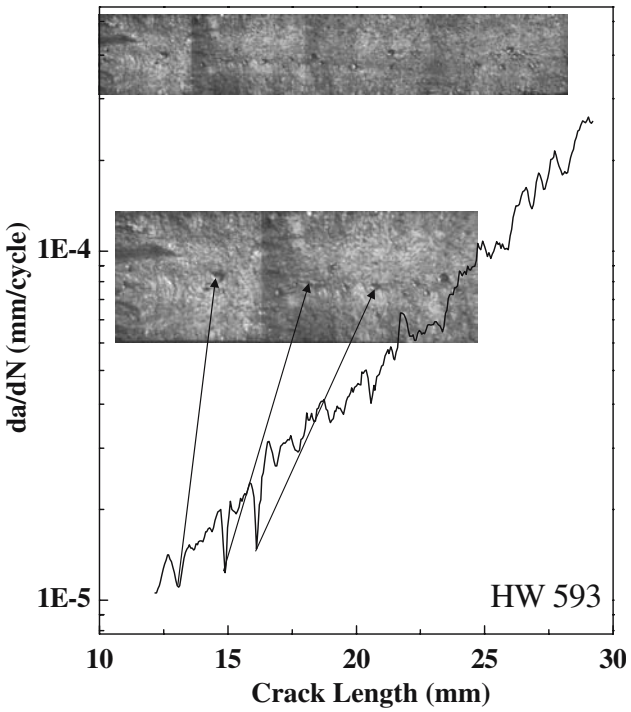

Fig. 4 Fatigue crack growth behavior of HW593 specimen with photographs showing the change of crack growth rate related with porosity

highly stretching the material ahead of crack tip resulted in a high crack opening. Such evidence could be responsible for reducing the beneficial effect of a locally dull notch tip. As a result, the serration and drop in FCGR took place sparingly at high R ratio. Invalid to traditional concept, the experimental result demonstrated that evenly distributed fine porosity in Ti–6Al–4V laser weld did not deteriorate its resistance to crack growth obviously. The strong lack of enhanced crack growth in Ti–6Al–4V weld with porosity could also be partly attributed to the facts that only a small fraction of fracture surface was covered with porosity, resulting in showing the crack growth behavior as a defect free weld.

Figure 5 is the SEM fractographs showing the typical fracture appearance of various specimens. The fatigue-fractured surface of the base plate showed transgranular fracture inter-dispersed with elongated quasi-cleavage fracture (Fig. 5a). A mixed mode fracture with coarse cleavage facets was found in the FZ of all welds (Fig. 5b). Irregular topography facets in the FZ indicated that the fracture process was aided by local brittle fracture along specific planes. Some of the facets even revealed a trace of acicular features, which could be related with the acicular martensite structure (Fig. 5c). On a macroscopic scale, the fatigue crack path is generally normal to the direction of external applied load. However, in microscopic view, the crack path often shows some deflection from the macro growth direction. Roughness-induced closure can be attributed to the crack path deflection, which is induced by the microstructure-sensitive crack growth [31]. A deflected crack tip not only reduces the local driving force for crack growth but also increases crack length, hence, prolongs the fatigue life or decreases the FCGR for a deflected crack [32, 33]. Within the same ΔK range, the crack path in the FZ was found to be more tortuous and irregular in nature as compared with the base plate. This observation was consistent with the rough fracture surface in the FZ relative to the base plate, as shown in Fig. 3. It can be deduced that the local cleavage fracture along specific plane of martensite in the FZ altered the crack growth direction significantly out of the primary crack plane, resulting in the reduced FCGR as compared to base plate at a given ΔK.

Figure 5d shows the surface morphology around the porosity and the variation of surface height determined by trace profile of SEM. Fatigue fracture appearance of porous weld did not show a great change in fracture morphology relative to that of defect free weld. However, the results indicated the fracture appearance around porosity showed a large variation in surface

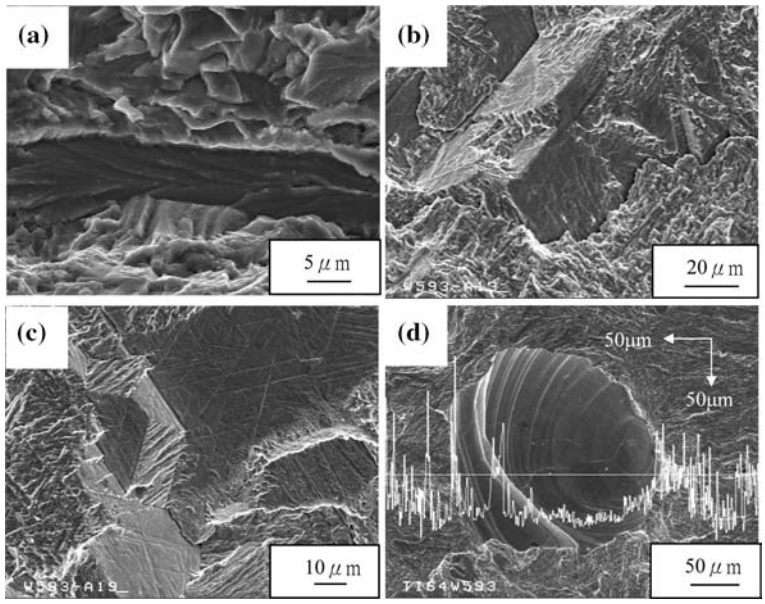

Fig. 5 SEM fractographs showing the fracture appearance of various specimens, (**a**) transgranular fatigue fracture interdispersed with elongated quasi-cleavage fracture in the base metal, (**b**) coarse cleavage facets in the FZ, (**c**) acicular features on the facet plane and (**d**) variation of surface height profile around porosity on the fracture surface

height from the normal plane of cracking. The highly varied fracture surface height also characterized an increased surface roughness or crack deflection. As the fatigue crack tip met the porosity, the local deflection of crack path associated with the high local rupture plasticity around porosity, accounted for a reduced FCGR in the porous weld as compared to the defect free weld at R 0.1. Besides, instant blunting of crack tip locally might also cause a reduction in the FCGR as the crack ran into porosity, resulting in the reduced FCGR around porosity therein. At high R ratio, such phenomena were less likely to occur and showed the behavior similar to a defect free weld. Such results could be partly attributed to the high R ratio to induce large crack opening.

Conclusions

The effect of a major welding defect viz., porosity, on FCGR in Ti–6Al–4V laser welds was investigated. Experimental results revealed that the porosity was present in the narrow FZ of the incomplete penetration welds. The FCGR of the FZ was significantly lower than that of the base plate. The fracture surface morphology of the welds was much rougher than that of the base plate. Randomly oriented martensite in the FZ leading to local cleavage fracture along specific plane of martensite, and altered the crack growth direction out of the primary crack plane. The zigzag crack path in the FZ resulted in the reduced FCGR at a given ΔK as compared to the base plate. Besides, the porous weld showed a serration on the crack growth curve, and behaved the similar crack growth characteristics as the defect free one. The combination of local tearing fracture with high plasticity around porosity and locally notch blunting as the crack tip pierced into porosity in the porous weld, compensated for the instant crack advance into the porosity, resulting in showing roughly the same FCGR as the defect free weld at R 0.1. Whereas, the serration and drop in FCGR occurred sparingly at high R ratio owing to a high crack opening.

Acknowledgements The authors gratefully acknowledge the financial support of this study by National Science Council of Republic China (92-CS-7-019-002). We also appreciate Dr. Raghu V. Prakash, Department of Mechanical Engineering, Indian Institute of Technology, Madras for his valuable suggestions and comments.

References

1. Thomas G, Ramachandra V, Nair MJ, Nagarajan KV, Vasudevan R (1992) Weld J 71:15s
2. Lancaster JF (1984) The physics of welding. Pergamon, Oxford, pp 269–290
3. Qi Huang G, Kullberg, Skoog H (1994) Optics Laser in Eng 20:3
4. Li Z, Gobbi SL, Norris I, Zolotovsky S, Richter KH (1997) J Mats Proc Tech 65:203
5. Thomas G, Ramachandra V, Nagarajan KV, Pant B, Sarkar BK, Vasudevan R (1989) Weld J 69:336s
6. Mazumder J, Steen WM (1980) Met Construct 12:423
7. Matsunawa A, Kim J, Katayama S (1997) ICALEO, Section-G, pp 73–82
8. Chen SJ, Devletian JH (1990) Weld J 69:319s
9. Chen SJ, Devletian JH (1982) Metall Trans 13A:865
10. Denney PE, Metzbower EA (1989) Weld J 68:342s

11. Yoder GR, Cooley LA, Crooker TW (1976) Metall Trans 8A:1937
12. Ravichandran KS (1990) Scripta Metall Mater 24:1275
13. Ravichandran KS, Dwarakadasa ES (1989) Scripta Metall 23:1685
14. Ravichandran KS, Dwarakadasa ES, Banerjee D (1991) Scripta Metall Mater 25:2115
15. Bache MR, Evans WJ, McElhone M (1997) Mater Sci Eng A 234–236:918
16. Evans WJ, Bache MR, McElhone M, Grabowski L (1997) Int J Fatigue 19:S177
17. Bache MR, Evans WJ (2001) Int J Fatigue 23:S319
18. Davidson DL, Lankford J (1984) Metall Trans 15A:1931
19. Irving PE, Beevers CJ (1974) Metall Trans 5:391
20. Yoder GR, Cooley LA, Crooker TW (1978) Metall Trans 9A:1413
21. Ogawa T, Tokaji K (1993) Fatigue Fract Eng Mater Struct 16:973
22. Fusion welding for aerospace applications, Aerospace material specification AMS-STD-2219A, May (1999)
23. Saxena A, Hudak SJ (1978) Int J Fracture 14:453
24. Tsay LW, Tsay CY (1997) Int J Fatigue 19:713
25. Shiue RK, Chang CT, Yang MC, Tsay LW (2004) Mat Sci Eng A364:101
26. Tsay LW, Yang MC, Chou FY, Shiue RK (2004) Mat Chem Phy 88:348
27. Shi YW, Chen BY, Zhang JX (1990) Eng Fract Mech 36:893
28. Beghini M, Bertini L, Vitale E (1994) Fatigue Fract Eng Mater Struct 17:1433
29. Kitsunai Y, Takana M, Yoshihisa E (1998) Metall Trans 29A:289
30. Nelson HG, Williams DP, Stein JE (1972) Metall Trans 3:469
31. Suresh S, Ritchie RO (1982) Metall Trans 13A:1627
32. Wang SH Muller C (1998) J Mat Sci 33:4509
33. Kamat SV, Eswaraprasad N (1992) Scripta Metall Mater 26:1713